DOUBLE ENDED GUILLOTINE BREAK IN A PRISMATIC BLOCK VHTR LOWER PLENUM AIR INGRESS SCENARIO

A Thesis

by

JESSICA LAUREN HARTLEY

Submitted to the Office of Graduate Studies of
Texas A&M University
in partial fulfillment of the requirements for the degree of

MASTER OF SCIENCE

August 2011

Major Subject: Mechanical Engineering

Double Ended Guillotine Break in a Prismatic Block VHTR Lower Plenum Air Ingress Scenario

DOUBLE ENDED GUILLOTINE BREAK IN A PRISMATIC BLOCK

VHTR LOWER PLENUM AIR INGRESS SCENARIO

A Thesis

by

JESSICA LAUREN HARTLEY

Submitted to the Office of Graduate Studies of
Texas A&M University
in partial fulfillment of the requirements for the degree of

MASTER OF SCIENCE

Approved by:

Chair of Committee, Yassin Hassan
Committee Members, William Marlow
Kalyan Annamalai
Head of Department, Jerald Caton

August 2011

Major Subject: Mechanical Engineering

ABSTRACT

Double Ended Guillotine Break in a Prismatic Block VHTR Lower Plenum Air Ingress Scenario. (August 2011)

Jessica Lauren Hartley, B.S., West Texas A&M University

Chair of Advisory Committee: Dr. Yassin Hassan

The double ended guillotine break leading to density-driven air ingress has been identified as a low probability yet high consequence event for Very High Temperature Reactor (VHTR). The lower plenum of the VHTR contains the core support structure and is composed of graphite. During an air ingress event, oxidation of the graphite structure under high temperature conditions in an oxygen containing environment could degrade the integrity of the core support structure. Following this large break, air from the reactor containment will begin to enter the lower plenum via two mechanisms: diffusion or density driven stratified flow. The large difference in time scales between the mechanisms leads to the need to perform high fidelity experimental studies to investigate the dominant air ingress mechanism. A scaled test facility has been designed and built that allows the acquisition of velocity measurements during stratification after a pipe break. A non-intrusive optical measurement technique provides full-field velocity measurement profiles of the two species particle image velocimetry. The data allow a more developed understanding of the fundamental flow features, the development of improved models, and possible mitigation strategies in such a scenario.

Two brine-water experiments were conducted with different break locations. Flow fronts were analyzed and findings concluded that the flow has a constant speed through the pipe after the initial lock exchange. The time in which the flow enters the lower plenum is an important factor because it provides the window of opportunity for mitigation strategies in an actual reactor scenario. For both cases the flow of the heavier density liquid (simulating air ingress from the reactor containment) from the pipe enters the reactor vessel in under 6 seconds.

The diffusion velocity and heavy flow front of the stratified flow layer were compared for the SF_6/He gas case. It is seen that diffusion plays less of a role as the transport mechanism in comparison to the density-driven stratified flow since the velocity of the diffusion is two orders of magnitude smaller than the velocity of the stratified flow mechanism. This is the reason for the need for density-driven stratified flow investigations following a loss of coolant accident.

These investigations provided high-quality data for computational fluid dynamics validation in order for these models to depict the basic phenomena occurring in an air ingress scenario.

DEDICATION

This thesis is dedicated to my dad (Texas A&M Centennial Class of 1976) who has been my inspiration to always pursue what I love and has always believed in me no matter what and to my mom (Texas A&M Centennial Class of 1976) who helps me realize there is more to life than work.

ACKNOWLEDGEMENTS

I would like to thank my committee chair, Dr. Hassan, and my mentor, Nate Salpeter, for their guidance and support throughout the course of this research.

I also want to extend my gratitude to the Nuclear Energy University Programs for supporting the work done for this project. Thanks also go to my friends and colleagues for their support and for making my time at Texas A&M University a great experience. Finally, thanks to my parents for their never ending encouragement and love through the course of my life that has led me to this point.

NOMENCLATURE

d_P	Particle Diameter (μm)
$D_{SF6\text{-}He}$	Diffusion Coefficient of SF_6-He (m^2/s)
dt	Change in Time (s)
dx	Change in Position (m)
Fr	Froude Number
g	Gravity Term (m/s^2)
g’	Reduced Gravity Term (m/s^2)
H	Hot Duct Diameter (m)
L	Diffusion Length (m)
$M_{SF6\text{-}He}$	Molecular Weight for the Binary Species (kg/kmol)
Ω_D	Diffusion Collision Integral
P	Pressure (atm)
ρ	Density of Fluid (kg/m^3)
ρ_{Heavy}	Density of Dense Fluid (kg/m^3)
ρ_{Light}	Density of Less Dense Fluid (kg/m^3)
ρ_P	Density of Seeding Particle (kg/m^3)
Ri	Richardson Number
$\sigma_{SF6\text{-}He}$	Entropy Generation (Angstrom)
T	Temperature (K)
T_{Diff}	Diffusion Time Scale (s)

μ	Viscosity (Pa*s)
u	Discharge Velocity (m/s)
u_{Heavy}	Flow Front Velocity of Heavy Density Fluid (m/s)
u_{Light}	Flow Front Velocity of Light Density Fluid (m/s)
U_g	Gravitational Velocity (m/s)
V_{Diff}	Diffusion Velocity (m/s)

Subscipts

g	Gravitational
m	Model
p	Prototype

TABLE OF CONTENTS

Page

ABSTRACT iii

DEDICATION v

ACKNOWLEDGEMENTS vi

NOMENCLATURE vii

TABLE OF CONTENTS ix

LIST OF FIGURES xi

LIST OF TABLES xiii

1. INTRODUCTION 1

    1.1 Very High Temperature Reactors 3
    1.2 Air Ingress Accident Scenario 5

2. LITERATURE SURVEY 8

    2.1 Air Ingress Investigations 8
    2.2 This Work 12

3. THEORY 13

4. SCALING ANALYSIS 16

5. EXPERIMENTAL APPROACH 20

    5.1 Experimental Set-up 20
    5.2 Visualization Techniques 22

6. UNCERTAINTY 29

    6.1 Experimental Uncertainty 29
    6.2 PIV Seeding Tracer Particle Uncertainty 32

Page

7. RESULTS AND DISCUSIONS 33

7.1 Liquid-liquid Air Ingress Investigations 33
7.2 Gas-gas Air Ingress Investigation 45

8. FUTURE WORK 49

9. SUMMARY AND CONCLUSIONS 50

REFERENCES 52

VITA 55

LIST OF FIGURES

FIGURE		Page
1	Department of Energy's Reference VHTR Schematic [1]	4
2	CFX Results of Two-Bulb Simulation with 16-mm Pipe [4]	9
3	Simplified 2-D Geometry of GT-MHR for Stratified Flow Simulation [5]	10
4	A Schematic Diagram of an Idealized Gravity Current	14
5	Air Ingress Test Facility	19
6	Isothermal Stratified Flow Experimental Setup	21
7	Schematic for the Isothermal Air Ingress Experiment	22
8	Brine-water Camera Setup for Long Pipe Case	25
9	Shadowgraphy in a Post Brine-water Experiment	26
10	Gas-gas Investigation Camera Setup for Long Pipe Case	28
11	Uncertainty Associated with the Field of View in Case A.	30
12	Uncertainty Associated with the Field of View in Case B.	31
13	Progression of Gravity Currents and Stratified Flow in Case A.	35
14	Progression of Gravity Currents and Stratified Flow in Case B	36
15	Experimental Results for the Pipe Flow Front Velocity versus Location in Case A	37
16	Experimental Results for the Pipe Flow Front Velocity versus Location in Case B	38
17	Experimental Results for the Pipe Flow Front Location versus Time in the Pipe	38

FIGURE Page

18 Highly Periodic Interfacial Instabilities between the Brine and Water..... 42

19 Experimental Results for Flow Front Location versus Time of the Lower Plenum..... 43

20 Experimental Results for Spreading Rate versus Location in the Lower Plenum..... 44

21 Zinc Stearate Particle Analysis (Ferro)..... 47

22 Zinc Stearate Particle Analysis (Struktol)..... 48

LIST OF TABLES

TABLE		Page
1	Fluids Used for Reactor Similarity	18
2	Camera Specifications	24
3	Description of Brine-water Investigations	34
4	Comparison of Flow Front Velocity between Experimental and Benjamin's Theoretical Model	39
5	Comparison of Flow Front Velocity between Experimental and CFD	40
6	Comparison of Diffusion Velocity to Density-driven Stratified Flow	46

1. INTRODUCTION

A new program for future nuclear energy systems, Generation IV, has been created in effort to provide next-generation technologies that will compete in all markets with the most cost-effective technologies expected to be available over the next three decades [1]. This program creates advantages which include reduced capital cost, enhanced nuclear safety, minimal generation of nuclear waste, and further reduction of the risk of weapons materials proliferation. One of the six reactor technologies considered under this program is the Very High Temperature Reactor (VHTR).

VHTRs are a part of the Next Generation Nuclear Plant (NGNP) or Generation IV reactors. The reactor core technology will either be a prismatic block or a pebble bed concept [1] with the cores composed of some type of fuel graphite cladding. The VHTR uses helium as coolant to produce core outlet temperatures in the range of 700-900°C. These higher temperatures generate higher power conversion efficiencies and provide high quality process heat for chemical processes, including hydrogen production. A level of passive safety is built into all the VHTR's conceptual designs for the next generation nuclear reactors [1]. Passive safety includes safety components which do not require active controller operational intervention to avoid accidents in the event of malfunction. Passive safety may rely on pressure differentials, gravity, natural convection, or the natural response of materials to high temperatures. Past studies have shown that density-

---

This thesis follows the style of Journal of Fluids Engineering.

gradient dominated stratified flow is an inherent characteristic of passive systems in advanced reactors [2] thus enabling VHTR's to be highly susceptible to this phenomenon.

In the VHTR, air ingress following a loss of coolant accident (LOCA) has been classified as being potentially one of the most severe accidents that can occur [2]. Air ingress occurs when a pipe connecting the reactor vessel and power conversion unit breaks and external air is allowed to enter the reactor vessel from the surrounding reactor cavity. The most catastrophic of these events occurs when there is a double ended guillotine break in the hot duct between the pressure vessel and the power conversion unit [2-4].

The double ended guillotine break leading to a gravity driven air ingress has been identified as a low probability yet high consequence event for VHTR. The lower plenum of the VHTR contains the core support structure and is composed of graphite [2, 3]. During an air ingress event, oxidation of the graphite structure under high temperature conditions could degrade the integrity of the core support structure. Following this large break, air from the reactor containment enters the lower plenum via two mechanisms: diffusion or density driven stratified flow. The large difference in time scales, and hence reaction time, between the mechanisms leads to the need to perform high fidelity experimental and numerical studies to investigate the dominant the air ingress mechanism. A scaled small test facility has been designed and built that allows the acquisition of velocity measurements during stratification and inflow/outflow behavior through a broken duct. Non-intrusive Particle Image Velocimetry (PIV) measurement

techniques provide full-field velocity measurements, and concentration profiles of the two species. These experiments provide new high fidelity full-field data of velocities and concentrations with high spatial and temporal resolution. The data allows for fuller concentrations with high spatial and temporal resolution. The data will allow for better understanding of the fundamental flow features, the development of improved models, and possible mitigation strategies in such a scenario.

1.1 Very High Temperature Reactors

The VHTR is one of the proposed reactor designs to play a role in future power generation. This reactor is one of six new reactor designs for the Generation IV reactor concepts. The main objective of the VHTR is cogeneration of electricity and hydrogen, as well as to other process heat applications. The major added benefits of the VHTR concept over previous reactors are higher thermal efficiency, hydrogen production, process heat applications, and high degree of passive safety [2]. The general schematic of the VHTR design is seen in Fig. 1. [1].

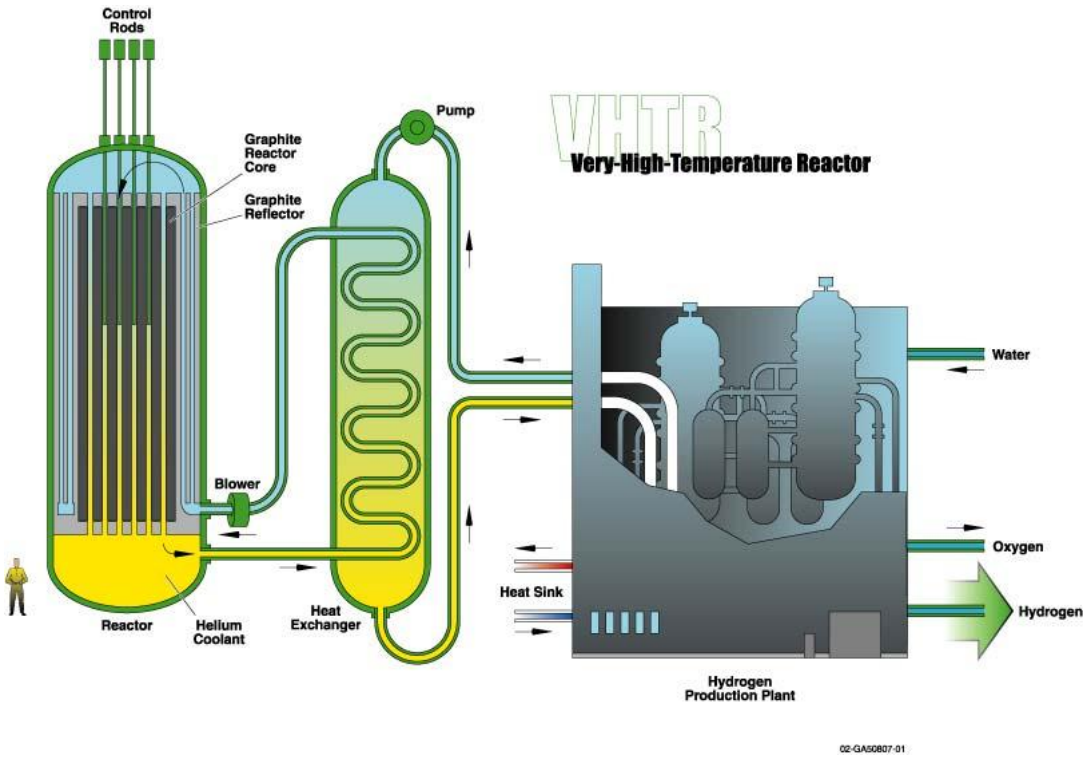

Figure 1: Department of Energy's Reference VHTR Schematic [1]

The basic technology for the VHTR has been well established in former High Temperature Gas Reactor (HTGR) plants, such as Dragon, Peach Bottom, and Fort St Vrain and is being advanced in concepts such as the Gas Turbine-Modular Helium Reactor (GT-MHR) and Pebble Bed Modular Reactor (PBMR) [1]. The VHTR is a helium gas-cooled, graphite-moderated, thermal neutron spectrum reactor with a core outlet temperature greater than 950°C [5]. These characteristics make the VHTR sufficient to support production of hydrogen by thermo-chemical processes. The preliminary reactor design is a 600MWth core connected to a steam generator to deliver

process heat [2]. This specific thermal power level is set to allow passive decay heat removal.

There are two configurations for the VHTR core: prismatic block or pebble-bed core. The main difference between the configurations is the geometry of the fuel. The main interest of this paper is the prismatic block core configuration. The prismatic core consists of an inner reflector region surrounded by an annulus of fuel blocks which is in turn surrounded by an annulus of outer reflector elements [6]. The basic fuel concept for the VHTR is TRISO coated particles which combined create compacts that fit into the fuel blocks. The fuel blocks are composed of hexagonal columns of graphite with circular holes coolant that run the full length of the column.

1.2 Air Ingress Accident Scenario

Prior literature pertaining to the air ingress accident scenario is initiated with a pipe break [2-6, 7, 8]. Immediately thereafter, depressurization begins and the hot helium coolant from the reactor vessel escapes. During this process, the helium mixes with the air in the external reactor cavity. Depressurization ceases and air ingress occurs when the pressure in the reactor vessel is equal to the pressure in the containment.

Initial studies focused on molecular diffusion as the primary ingress mechanism with a time scale of around 150 hours [2]. However, recent studies have shown that assuming molecular diffusion as the driving factor in air ingress is physically incorrect. Instead, the primary mechanism for air ingress is shown to be a gravity driven process that occurs due to the large density difference between the internal helium coolant and

the external helium-air mixture following a break. The different densities result in a gravity driven flow between the cooler, higher density helium-air mixture in the containment and the hotter, lower density helium present in the reactor vessel. A counter-current exchange flow similar to that modeled by Benjamin's equation [1, 9] occurs and the time scale for helium-air mixture to penetrate the lower plenum is expected to be less than 10 seconds depending on break location. The main difference in this presented research case from the previous Benjamin study [9] is that the duct is cylindrical rather than rectangular. Further differentiation of this work from previous air-ingress studies is the presence of a co-annular duct at the break. This duct used in this study is geometrically scaled to model the General Atomics Gas Turbine-Modular Helium Reactor (GT-MHR) [2]. As the gravity driven flow enters the lower plenum region of the vessel, the helium-air mixture begins to heat up at which point natural convection is thought to take place as the now heated mixture begins to rise and drive cooler gasses down the walls of the reactor vessel and out through the cool duct.

Because of the differing time scales of interaction, the primary air ingress mechanism, whether it is dominated by diffusion or density driven stratified flow needs to be verified. Air ingress may result in the oxidation of in-core graphite structures and fuel. Although the amount of oxygen present in the containment is unlikely to cause oxidation to the point of collapse, superficial oxidation of support structures and core materials may result in significant dust generation and resulting fission product release as flows entrain ash particles off the graphite surfaces. By understanding the full cycle of

the air ingress scenario through careful experimentation, mitigation strategies may be developed for such an accident.

2. LITERATURE SURVEY

2.1 Air Ingress Investigations

To obtain a thorough understanding of the physical phenomena that occurs during a LOCA of a VHTR and for the air ingress scenario as a whole a survey of literature needed to be conducted. The methods and results of various air ingress accident scenario simulations and experiments for LOCA in VHTRs are presented in the following section.

Numerical studies were conducted by Idaho National Laboratory (INL) on Duncan and Toor's [10] two bulb studies using GAMMA and CFX [4]. Duncan and Toor's two bulb studies consist of two bulbs connected by a small diameter pipe of 2.08 mm. One bulb is filled with a heavier gas, CO_2 (simulating the ingress of air into the reactor), and the other with a lighter gas, H_2 (simulating the reactor coolant). The bulbs are closed to one another prior to the start of the experiment. In this numerical study the exact dimensions of the experimental equipment were used. The findings reveal that the small pipe molecular diffusion is a main phenomenon for gas transport. Findings show that diffusion is a slow process. Even after 200 seconds the gas concentrations of the lighter gas bulb and the heavier gas bulb are not changed [4]. For the second numerical study conducted in 2009 at INL [4], the same dimensions were used as in the experiment and the diffusion two bulb analyses except for the diameter of the capillary tube. The capillary tube was changed to a diameter of 16 mm. Figure 2 shows the simulation after 30 seconds and depicts the heavier gas CO_2 flows to the bottom and the lighter gas

hydrogen is on top of the heavier gas. This indicates that the density-gradient-driven stratified flow is a dominant phenomenon for the gas species in a larger size pipe of 16 mm [4]. This reveals the large time difference in the two ingress mechanisms and indicates that further investigation is needed when a LOCA occurs in a VHTR.

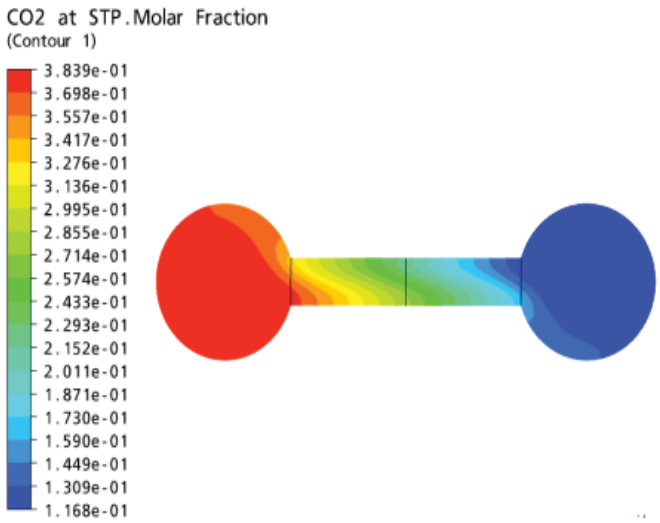

Figure 2: CFX Results of Two-Bulb Simulation with 16-mm Pipe [4]

To further the investigation of the air ingress mechanism, INL performed a preliminary numerical study on the stratified flow phenomena in the VHTR LOCA [5]. This study was investigated using FLUENT 6.3 using a 2-D model of GT-MHR 600MWt reactor reference geometry. This 2-D model was constructed with 5 major zones as seen in Fig. 3 with the size of the reactor cavity not being taken into account.

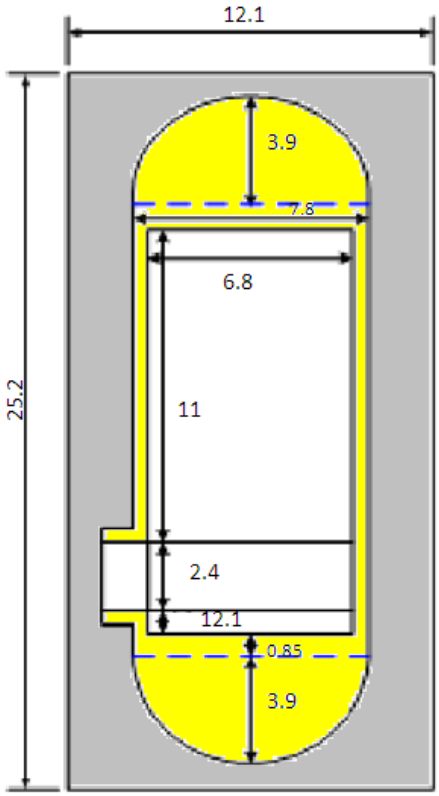

Figure 3: Simplified 2-D Geometry of GT-MHR for Stratified Flow Simulation [5]

The investigation revealed that air ingresses rapidly into the reactor core with counter-current stratified flow shape [5]. In this calculation, it only took 60 seconds for the air to fill up the lower plenum and to stabilize. This time scale is instantaneously small compared to the whole air ingress time frame that was found for the diffusion ingress mechanism (~150 hrs) [5].

In efforts to estimate the consequences of the stratified flow assumption as the air ingress mechanism, INL performed another numerical investigation. This investigation examines the whole air ingress scenario using both Fluent and GAMMA codes [2]. The

main purpose for this investigation was to understand the stratified flow effect as air ingresses into the reactor and to find the onset of natural convection. The GT-MHR was used as the reference geometry and the Fluent simulations reveal that natural convection was initiated 160 seconds after stratified flow was started and also the whole reactor vessel was filled with air after 4 minutes [2]. This accelerated onset of natural convection leads to much faster oxidation in the graphite structures. The conclusion (new assumption-stratified flow) was that air ingress is a much more severe than previously thought and the previous assumption on air-ingress accident will lead to the underestimation on their consequences. It is therefore recommended by INL that the original air-ingress scenario based on molecular diffusion be replaced with the new assumption considering stratified flow.

Studies on density-gradient-driven stratified flow in advanced reactor systems has been the subject of active research for over a decade because density-gradient dominated stratified flow is an inherent characteristic of passive systems used in Light Water Reactors (LWR) [7]. Liou, 2007 performed density driven stratified flow experiments using water as the working fluid instead of helium. In one experiment he used air, oil, and water to develop a visualization of the role density plays on varying fluids in a pipe. The LWR is conceptually identical and directly applicable to the phenomenological behavior that occurs in the NGNP. The governing equations from this experiment are identical to the ones used in the air ingress event of a VHTR [7].

In 2010, Oh and Kim [8] conducted experiments to investigate density driven stratified flow during a LOCA of a VHTR. The experiments were conducted in two

acrylic tanks connected by a pipe using brine and water as the working fluids. The fluids were separated by a large valve to simulate the pipe break and the facility was scaled down model of a GT-MHR as the reference reactor. The isothermal experiments had two objectives:

1) to understand stratified flow phenomena in the VHTR and

2) to provide experimental data for validating computer codes.

The experiment shows clear stratified flow between the heavy and light fluids. Also, Benjamin's model provides a good prediction for flow front speed for internal stratified flow. This model was used as a comparison to the experimental data in which less than 10% error was found [8].

All of these investigations provide insight into the air ingress scenario. Without knowing what has been done in the past, nothing can be improved in the future.

2.2 This Work

In this work, experiments were performed to investigate the dominant air ingress mechanism during a LOCA. A small scaled test facility was designed and built to allow the acquisition of velocity measurements during stratification and inflow/outflow behavior through the broken duct. Investigations include two shadowgraphy investigations with different pipe break locations and one Particle Image Velocimetry (PIV) investigation.

3. THEORY

Density driven currents, or often called gravity driven currents, are induced by density variations due to a difference in temperature, presence of a dispersed solid phase, or heavier dense gas. Lock exchange flows are a class of density currents in which surface tension can be neglected and counter current flows are produced. These are simple flow configurations, which may, however, result in very complex flows characterized by physical processes such as the emergence of Kelvin-Helmholtz-like instabilities, the formation of lobes and clefts at the front leading edge, etc [11].

Lock exchange flows consists of two fluids of different densities initially separated by a gate. When the gate is removed, differences in the hydrostatic pressure cause the denser fluid to flow in one direction along the bottom boundary of the tank, while the lighter fluid flows in the opposite direction along the top boundary of the tank [12]. A basic configuration of the flow is shown in Fig. 4.

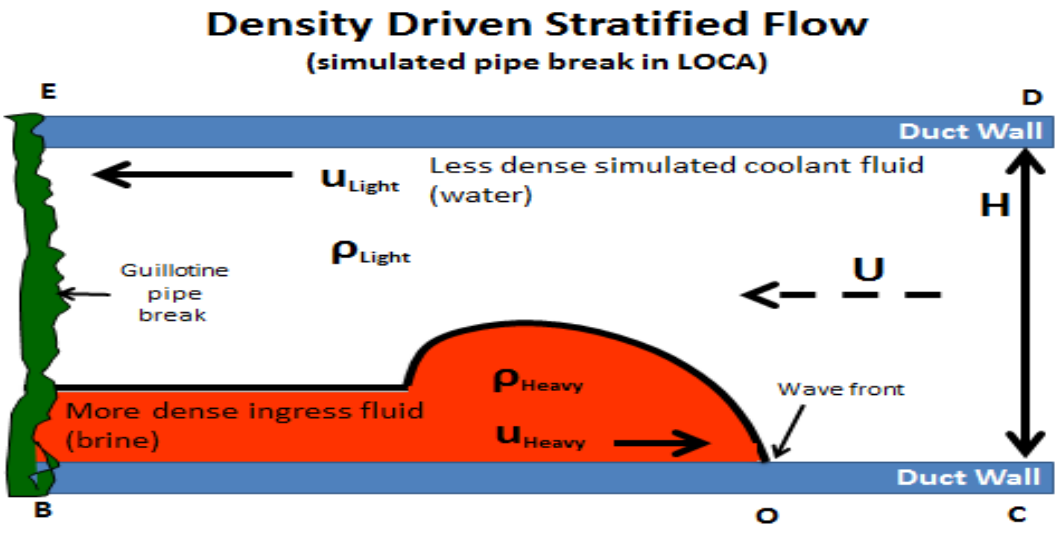

Figure 4: A Schematic Diagram of an Idealized Gravity Current

The rectangular block was the first agreed upon assumption of many investigators of lock exchange flow. The major assumption in the approximation is that it follows inviscid fluid theory. By equating decreasing potential energy to increasing kinetic energy, the following result is obtained [13]:

$$\frac{U_{Heavy}}{\sqrt{(g'H)}}=0.5 \quad (1)$$

Experiments revealed a very close value to be 0.44.

The inviscid fluid theory provides a useful approximation to the behavior of a gravity current front. This theory assumes no viscous forces are present. Benjamin [9] analyzed the front of a frictionless gravity current. The Benjamin model was used in this paper to analyze the flow front.

Lock exchange flow progresses in three stages [14]:

1) After the initial collapse of fluid when the gate is removed there is an adjustment phase in which the front advances at constant speed.
2) The second stage is self- similar flow in which the gravity current is collapsing. The current depth is decreasing with time.
3) The third stage comes in effect if viscous effects become dominant.

Most of the mixing within the density current occurs in the front, or often called the head of the current. The mixing has two major effects on the transport of the dense fluid [15]:

1. It locally increases the internal near bed velocity of the flow with respect to the front propagation rate.
2. It increases the total amount of fluid transported for known current characteristics.

There are two dominant types of instabilities that are responsible for mixing that occur in density currents, billows and clefts and lobes. Billows are an instability that rolls up in the region of velocity shear above the front of the dense fluid. A certain type of billow that is explored is the Kelvin Helmholtz instability. This instability is formed at the interface between two fluids of different density moving relative to each other. The complex shifting pattern of clefts and lobes are formed by the influence of the ground or bottom of the tube on the lower part of the edge [14].

4. SCALING ANALYSIS

To validate the fact that the scaled down laboratory scale experimental apparatus effectively simulates conditions expected in the VHTR, this section discusses the scaling analysis for air ingress via density driven stratified flow phenomenon in the experimental simulation of the VHTR during a LOCA. This section identifies the respective dimensionless groups and similarity criteria used to describe this phenomenon.

Scaling analysis was performed for the density driven stratified flow phenomena in a VHTR. Commonly used dimensionless numbers to characterize stratified flow are Richardson and Froude numbers under the Boussinesq approximation. The essence of the Boussinesq approximation is that the difference in inertia is negligible but gravity is sufficiently strong to make the specific weight appreciably different between the two fluids.

In the scaling analysis, the flow front velocity of the light and heavy fluids are assumed to closely follow Benjamin's equation, Eq. (2) and (3), based on previous studies with a single cylindrical pipe [9]. The dimensionless numbers are matched in the model and prototype with a reduced gravity term, Eq. (4) and are set to unity as seen in Eq. (5) and Eq. (6).

$$u_{Heavy}=0.44\sqrt{g'H} \tag{2}$$

$$u_{Light}=0.44\sqrt{gH(\rho_{Heavy}-\rho_{Light})} \quad (3)$$

$$g'=g\frac{\rho_{Heavy}-\rho_{Light}}{\rho_{Avg}} \quad (4)$$

$$\frac{Ri_m}{Ri_p}=\frac{u_p^2 g_m' h_m}{u_m^2 g_p' h_p}=1 \quad (5)$$

$$\frac{Fr_m}{Fr_p}=\frac{u_m\sqrt{g_p' h_p}}{u_p\sqrt{g_m' h_m}}=1 \quad (6)$$

As seen in the previous equations, the Froude number (Fr_m/Fr_p) is the ratio of inertial forces to gravitational forces and the Richardson number (Ri_m/Ri_p) is the ratio of potential energy to kinetic energy. Both are highly dependent on the density ratio and the characteristic length scale (H). With the scaled down experimental test facility and the resulting scaled down characteristic length, there was a need to adjust the density ratio to obtain the necessary Froude and Richardson numbers that represent reactor conditions during a LOCA to provide representative results. To accomplish this, different fluids were used to adjust the density ratio to obtain the same dimensionless numbers as in the actual reactor. The density ratio for the actual reactor is 0.14 and to obtain this same ratio a variation in concentrations for the fluids are used. These fluids are found in Table 1.

Table 1: Fluids Used for Reactor Similarity

Fluids Used	**Froude Number**	**Richardson Number**	**Density Ratio ($\rho_{light}/\rho_{heavy}$)**	**Flow Front Velocity Ratio (u_{heavy}/u_{light})**
Helium-Air (Reactor)	0.33	0.68	0.14	2.69
Water-Brine	0.43	4.89	0.88	1.06
Helium-SF6	0.33	0.68	0.14	2.69
Helium-CO2	0.33	0.87	0.14	2.69

Although not all the fluids listed in Table 1 are of the same density ratio and dimensionless numbers, each fluid combination played a specific purpose.

- The air ingress facility was scaled using sulfur hexafluoride (SF_6) and helium as the working fluids. These two fluids match the dimensionless numbers and density ratio which in turn allows the flow front velocity ratios to be the same that occur in the actual air ingress scenario of the reactor.
- Carbon dioxide and helium will be used as a comparison to the sulfur hexafluoride-helium case with matching Froude number, density ratio, and flow front velocity ratios. Even though the Richardson number was not matched in this case due to the different densities, this case provides a good prediction of flow during the air ingress scenario.
- The brine-water case acts merely as a flow visualization to capture important points prior to first testing and as initial validation to CFD results of the

brine-water case. The brine-water case does not match the dimensionless numbers as in the reactor due to the fluids needed for the flow visualization. Prior to the flow visualization experiment, the density of the brine solution and water were measured by a hydrometer and the viscosity measured by a rheometer to ensure accurate estimates of the flow front velocity. These dimensionless parameters along with the Reynolds number were used to calculate the flow regime.

From this scaling analysis, a test facility was constructed to faithfully represent the density driven stratified flow phenomenon as seen in Fig. 5. From geometric scaling, this test facility is approximately 1:20 length scale of the actual reactor size.

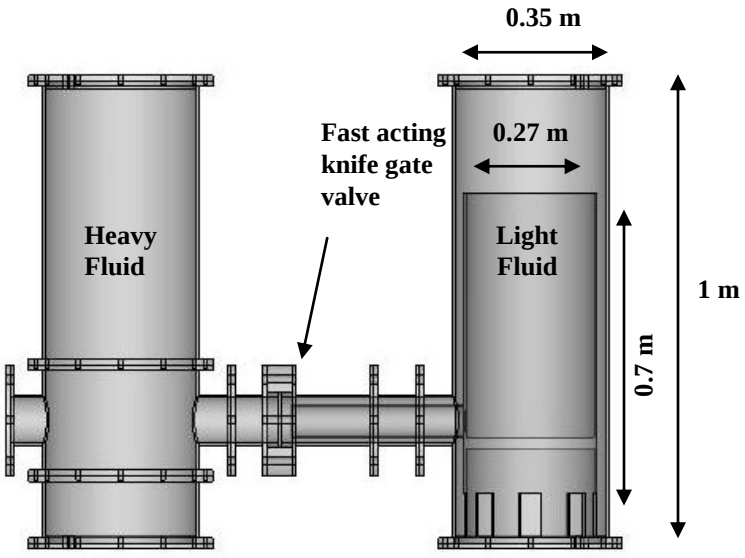

Figure 5: Air Ingress Test Facility

5. EXPERIMENTAL APPROACH

5.1 Experimental Set-up

The isothermal stratified flow experiment consists of two acrylic tanks and a horizontal coaxial pipe connecting the two tanks as seen in Fig. 5. The inner pipe has a diameter of 0.066 m and the outer pipe has a diameter 0.1 m with a length of 1.0 m. The tanks have a diameter of 0.35 m, and a height of 1.0 m. The heavy fluid tank that simulates the reactor vessel has an inner tank to simulate the reactor core. This inner tank has a diameter of 0.29 m and a height of 0.7 m.

Both the tanks and the coaxial pipe are made of a transparent acrylic for optical measurements and flow visualization. Along the horizontal coaxial pipe is a sliding knife gate valve (Dezurik Knife Gate Valve, KGC, 5, F1, S1, TDP, S1-CR*CY-PC6, 4V1045) installed to separate the tanks, which can be seen in Fig. 6. Initially, both tanks were filled with fluids having different densities, and the valve was closed. To initiate the experiments, the valve was quickly opened (simulating a guillotine break) with 80 psi compressed air. As a result of the break, a counter-current stratified flow formed in the test-section where the heavy fluid intruded into the light fluid at the bottom of the tank, and the light fluid intruded into the heavy fluids at the top of the tank.

Figure 6: Isothermal Stratified Flow Experimental Setup

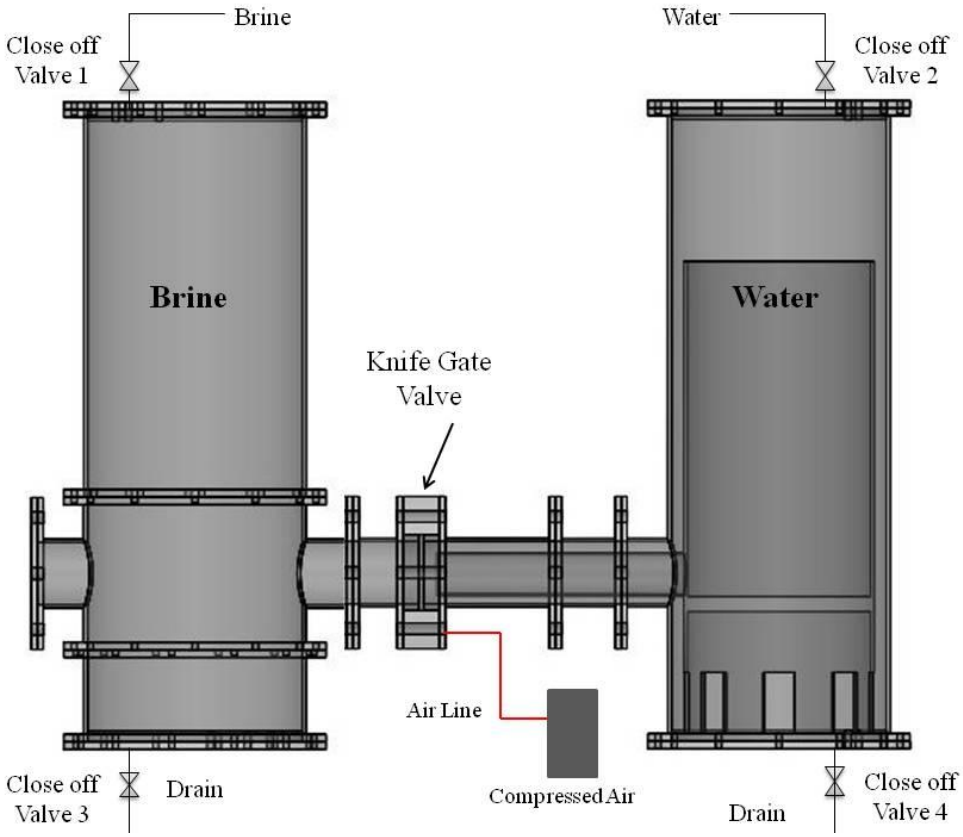

Figure 7: Schematic for the Isothermal Air Ingress Experiment

5.2 Visualization Techniques

Several visualization techniques were used to analyze the density driven stratified flow front in the simulated air ingress scenario of a VHTR during a LOCA. Among these techniques were Shadowgraphy and Particle Image Velocimetry (PIV).

5.2.1 Shadowgraphy, Setup, and Flow Measurement

Initial flow visualization tests were conducted using a brine solution to simulate the heavy helium-air mixture in the reactor containment, and water to simulate the hot

helium exiting the reactor vessel. Flow visualizations using shadowgraphy techniques were conducted to investigate the stratified flow that occurs following a pipe break. Shadowgraphy is an optical method that depicts fluid flow patterns made visible by using differences in index-of-refraction in the flow. The fluid is illuminated by a beam of light which bends toward regions of higher refractive index while passing through a transparent material. In our experiment, the light beam used in shadowgraphy is the LEC light source which provides a monochromatic source of light.

Shadowgraphy was used to measured the relative flow front velocity in the pipe as it progresses into the lower plenum. To accomplish this, two fluids, a dyed brine solution and water were used with a fast actuating knife gate valve to simulate the pipe break. High speed cameras captured the flow of the two fluids in the pipe as it entered the lower plenum. Figure 7 shows the schematic for the isothermal air ingress experiment. Initially, the knife gate valve is closed and valves 3 and 4 are closed. The brine solution is mixed prior to experiment and dye is added. The density and viscosity are measured prior to experiment with a hydrometer and viscometer respectively. The water and brine solution is added to respective tanks filling through the feed lines into through valves 1 and 2. The pneumatic knife gate valve is pressurized with 80 psi of compressed air and is opened by turning on a switch. The flow pattern is captured in the horizontal coaxial pipe by high speed cameras. After the experiment, the power source to the knife gate valve is de-energized and valves 3 and 4 are opened to discharge the fluids to be discarded.

To capture the flow, one to two high speed cameras (number depends on length of pipe) are placed perpendicular to the pipe interrogation region depending on the break location and another camera is placed on top of the tank that symbolizes the reactor vessel to capture flow propagation entering the lower plenum. The break location varies which changes the length of the pipe. This creates a need for different number of cameras to capture the flow front. Figure 8 shows the camera set-up of the flow visualization for the brine-water investigation. The camera specifications used for this investigation are given in Table 2.

Table 2: Camera Specifications

	Camera 1	**Camera 2**	**Camera 3**
Location	Viewing co-annular pipe from the front (blue box)	Viewing co-annular pipe from the front (red box)	Viewing reactor vessel lower plenum from above
Make	Vision Research	Phantom	Vision Research
Model	v7.3	Ultima-ATX	v7.3
Max. Resolution	800x600 pixels	1024x1024 pixels	800x600 pixels
Frame Rate	6688	2000	6688
Optics	Carl Zeiss Makro-Planar T* 2/50		

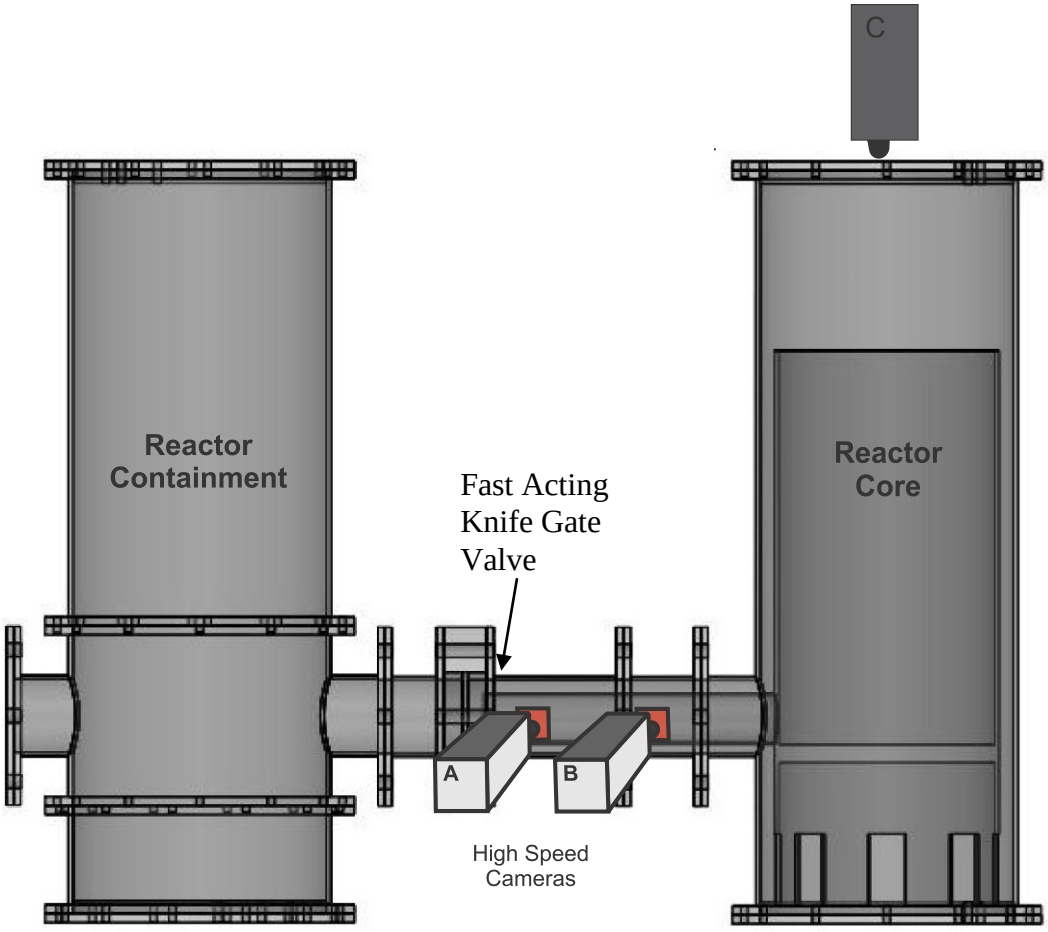

Figure 8: Brine-water Camera Setup for Long Pipe Case

Figure 9 shows the backlight illumination source used for the shadowgraphy in a post brine-water experiment. A flexible 36”x12” Ceelite light emitting capacitor (LEC) provided monochromatic illumination along the length of the pipe and a round 12” LEC was used below the simulated reactor vessel to provide illumination for the tank camera (Camera 3).

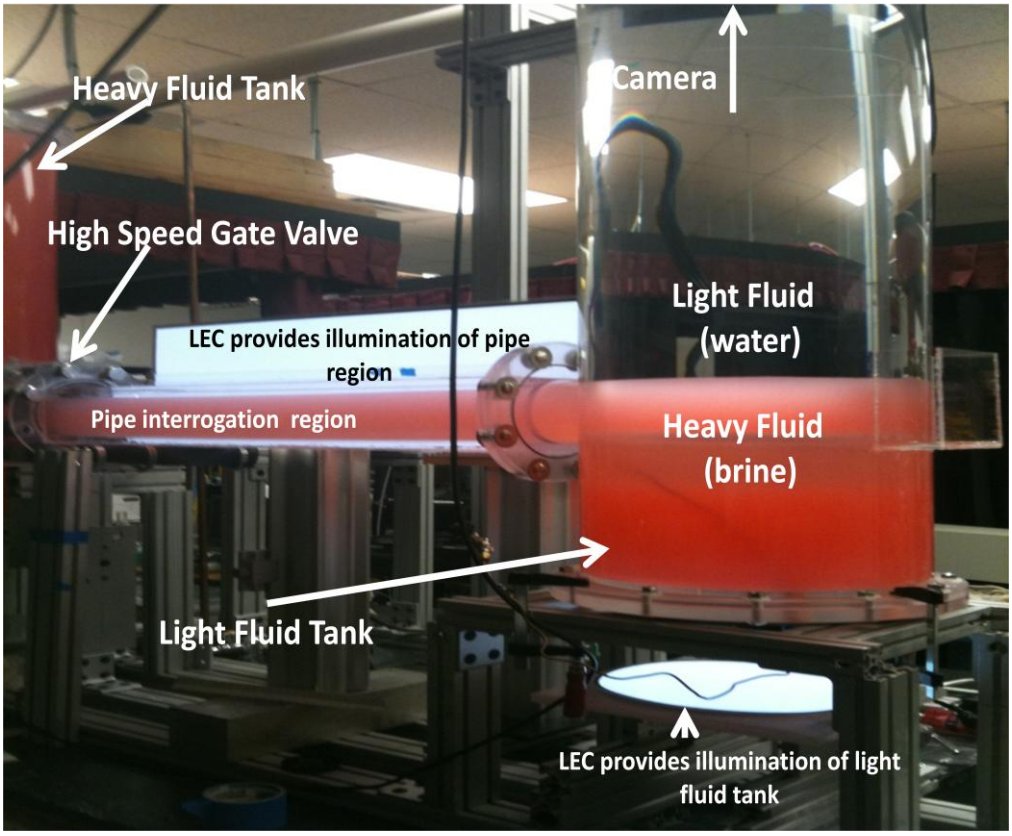

Figure 9: Shadowgraphy in a Post Brine-water Experiment

Flow front velocity measurements were conducted using one to two high speed cameras at the pipe and spreading rate measurements were conducted using one camera over the simulated reactor tank (light water tank in Fig. 8). Each camera has a known frame rate (Table 2). Prior to the experiment, the distance from the guillotine break along the tube is measured and marked. These distance measurements are used to measure the wave front travel as it propagates down the tube. With the use of image

processing software, the change in distance of the wave front is correlated with the number of frames to determine the wave front travel time. The comparison of the travel time with the travel distance along the tube provides the wave front velocity.

5.2.2 Particle Image Velocimetry (PIV) Technique, Setup, and Flow Measurement

Particle Image Velocimetry (PIV) is a non-intrusive optical measurement technique that provides full-field quantitative and qualitative information of the flow with high spatial and temporal resolution. The measuring principle is based on the fact that instantaneous fluid velocities can be measured by recording the position of images produced by small tracers suspended in the fluid, at successive time increments.

PIV methods inherently measure the Lagrangian velocities of the tracer particles [16]. The underlying assumption is that these tracer particles closely follow the fluid motion with minimal lag. This assumption holds true for a wide variety of flows of interest, provided that the tracers are small enough and/or their density approaches that of the fluid. To improve measurement accuracy of the flow velocity, PIV needs a high concentration of tracers with the measurement of the "local" fluid velocity being obtained from an average over many tracers contained in a measurement volume.

Experiments were performed in a specially designed small test facility that allowed the measurement of the velocity and the temperature during stratifications and as a result evaluate the inflow/outflow behavior through the broken duct. The experimental setup for PIV investigations of gas-gas scenarios is seen in Fig. 10. The visualization system consisted of particles flow tracers, a high-speed high-resolution camera, a high-power laser, a continuous halogen lamp, mirrors, translational stages, and

lenses. These experiments provided full-field data of velocity with a high degree of spatial and temporal resolution. The analysis of the data provided an understanding of the fundamental flow features which could lead to improved CFD models the air ingress scenario.

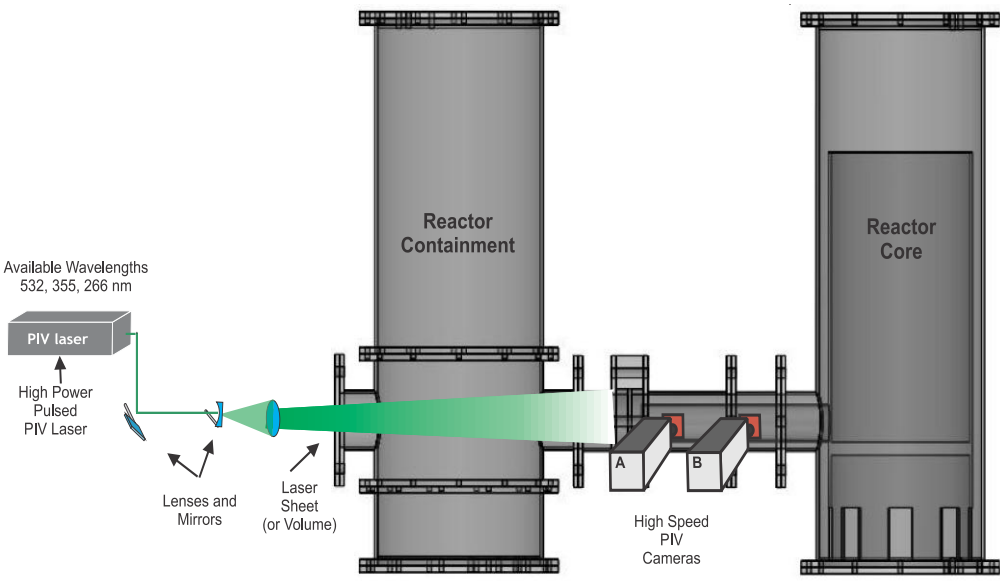

Figure 10: Gas-gas Investigation Camera Setup for Long Pipe Case

6. UNCERTAINTY

6.1 Experimental Uncertainty

This section identifies uncertainties associated with field of view errors in the flow visualization investigations. For both case A and case B, uncertainties arise when measuring flow front velocity. The cameras are lined up to catch the flow after the pipe break and the flow as it propagates down the investigation region of the pipe (these investigation regions are different for both cases and are specified in Figs. 11 and 12). The cameras are aligned to the edge of the pipe and measurements of the flow front occur from the middle of the pipe. Therefore the maximum uncertainty occurs at the edge of the pipe where the flow front is at the widest angle.

Uncertainty measurements were calculated by measuring the angle projected by the field of view and the pipe. This angle was then used to calculate the skewed length from where the flow front measurements are taken place. The maximum uncertainty is calculated using Eq. (7).

$$\text{Max.Uncert.} = \frac{\text{Skewed Region}}{\text{Investigation Region}+\text{Skewed Region}} \tag{7}$$

Schematics of these uncertainty measurements are seen in Fig. 11 and 12.

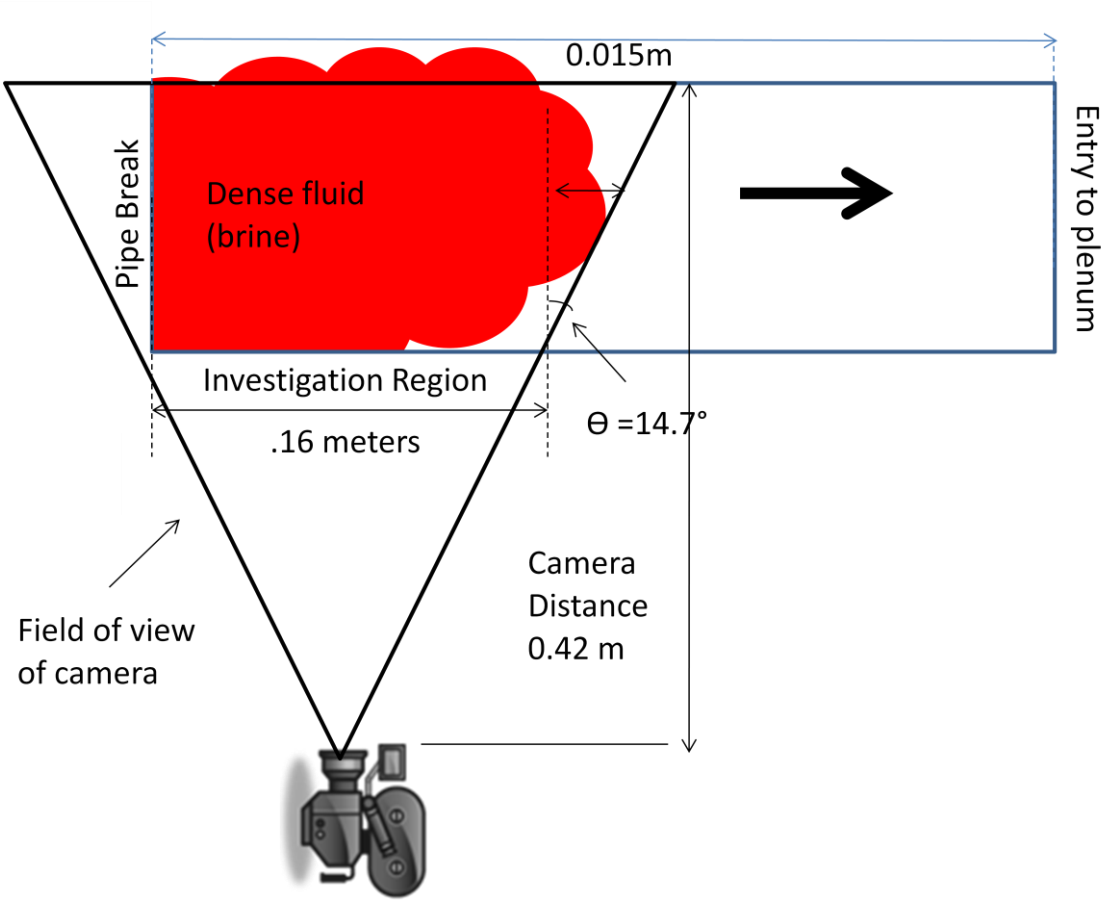

Figure 11: Uncertainty Associated with the Field of View in Case A

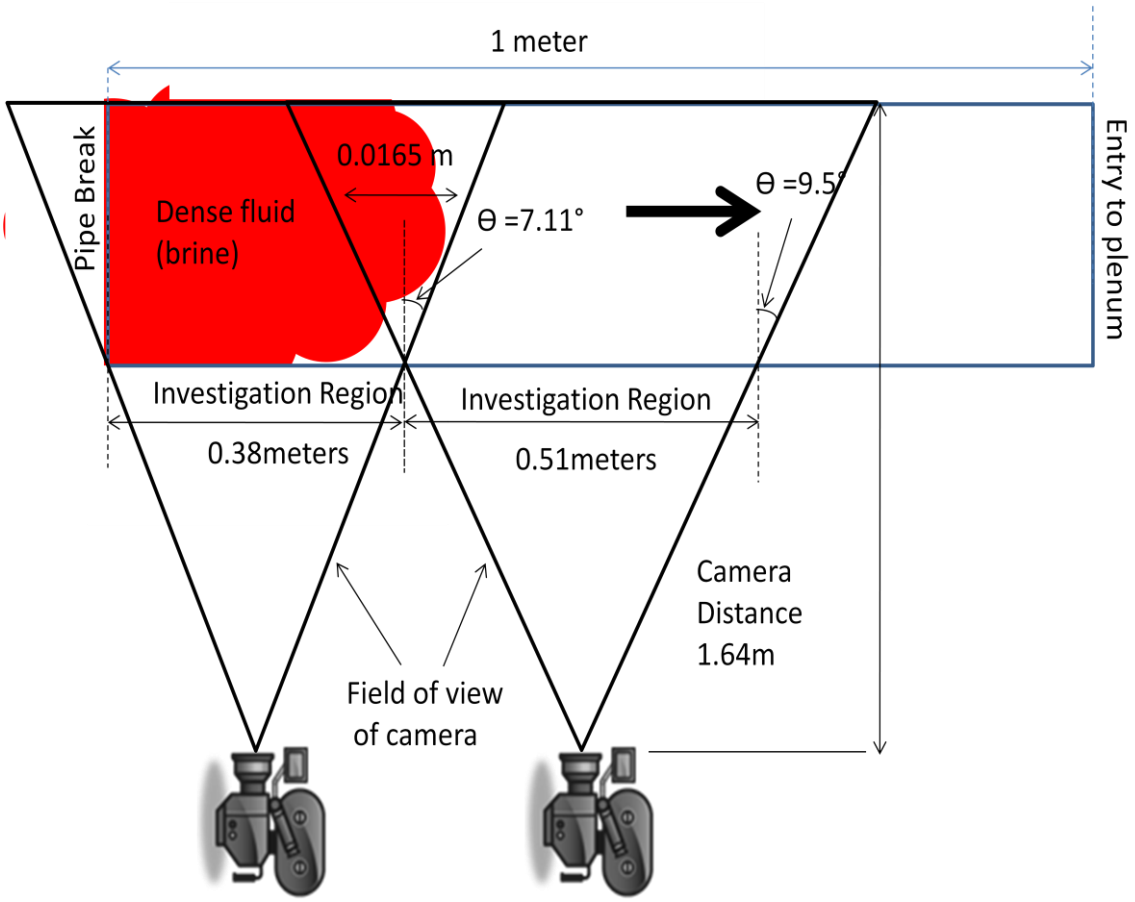

Figure 12: Uncertainty Associated with the Field of View in Case B

Case A was found to have a maximum uncertainty of 4.29% due to the angle of 14.7° skewed angle. Case B utilized two cameras which both have their own uncertainty associated with the angle. Case B was found to have a maximum uncertainty of 1.8% and 1.89% respectively of the two cameras due to the skewed angles of the two cameras used. These two uncertainties for Case B were combined to get the maximum

uncertainty of 3.69%. All of the uncertainties were propagated to the velocity calculations.

6.2 PIV Seeding Tracer Particle Uncertainty

On the PIV measurements, a source of error is induced by gravitational forces if tracer particles' density differs largely from that of the fluid. An indication whether gravitational forces becomes important can be obtained from Stokes drag law [17], from which the gravitational induced velocity U_g is given by

$$U_g = d_p^2 \frac{(\rho_p - \rho)}{18\mu} g \tag{8}$$

where d_p and ρ_p are diameter and density of the particles, ρ and μ are the density and dynamic viscosity of the fluid, and g is the gravitational acceleration. In the PIV investigation for air ingress seen in this work, sulfur hexafluoride (SF_6) is the gas used for the working fluid and zinc stearate as the tracer particle used to monitor its flow through the tube. The large density difference is the main drive for this initial calculation. In this investigation the fluid density gradient induced a maximum gravitational velocity of U_g=50 μm/s in comparison to the initial calculation using the Benjamin equation of 1.29 m/s flow speed of the SF_6 gas. Therefore the influence of fluid density changes on velocity estimation can be neglected.

7. RESULTS AND DISCUSSION

The flowing section describes separate effect experiments for understanding stratified flow phenomena in the air ingress accident scenario and the data generated for validation of CFD codes. The experiment investigates density driven stratified flow in an air ingress scenario following a double ended guillotine break (DEGB) of the large pipe connecting the reactor and the steam generator.

Three investigations were performed to develop an understanding of this stratified flow phenomenon: two liquid-liquid investigations using shadowgraphy to study the effects of varying pipe break locations and one gas-gas investigation utilizing PIV. The three experiments investigate the flow front as it propagates though the pipe after the break. In addition, the lower plenum spreading rate is investigated in the liquid-liquid scenario.

7.1 Liquid-liquid Air Ingress Investigations

Liquid-liquid investigations are important to help understand important flow features dominant during an air ingress scenario in the scaled down experimental facility used in this investigation. The liquids used for this investigation were brine, used as the heavy working fluid (representing air ingress from reactor containment), and water as the light working fluid (representing the loss of hot coolant from the reactor core). Two investigations were conducted to investigate the effect of pipe break location. The pipe break locations are characterized based on the length of coaxial pipe that connects the

simulated reactor tank to the valve. Table 3 provides a description of the pipe length cases investigated. Camera 1 captured the pipe region extending to 0.51 m and was adequate by itself for Case A. Because of the increase pipe length, case B required the use of two cameras to capture the flow front propagation through the pipe. Camera 1 investigation region of 0.51 m plus Camera 2 investigation region of 0.38 m with a total investigation region of 0.89 m.

Table 3: Description of Brine-Water Investigations

	Density Ratio ($\rho_{light}/\rho_{heavy}$)	**Pipe Length (m)**	**Investigation Region (m)**
Case A	0.88	0.38	0.16
Case B	0.88	1.0	0.89

7.1.1 Flow Front Analysis

From the initial flow visualizations, the flow front was captured in the pipe and entering the lower plenum. Figures 13 and 14 shows the heavy fluid current propogating through the pipe after the valve is opened in both cases. As can be seen the density driven stratified flow model introduced in Fig. 4 appears to approximate fairly well the experimental results in this investigation. From this, the flow front speed in the coaxial pipe and spreading rate into the lower plenum was calculated. These visualizations provide insight to the short time scale it takes for a heavy fluid to move from the

initiated pipe break through the pipe to the reactor and potentially cause an earlier onset of oxidation (on the order of a tens of seconds).

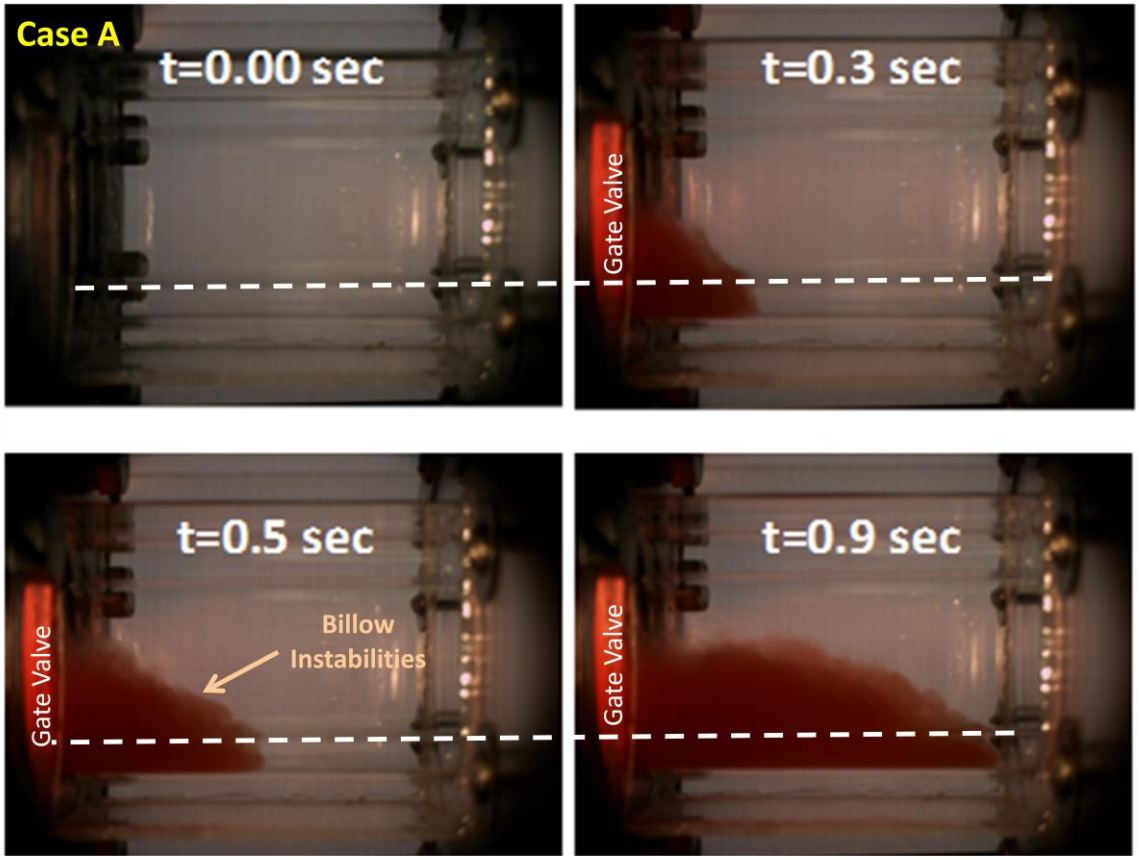

Figure 13: Progression of Gravity Currents and Stratified Flow in Case A. The Dashed Line Signifies the Inner Pipe Location

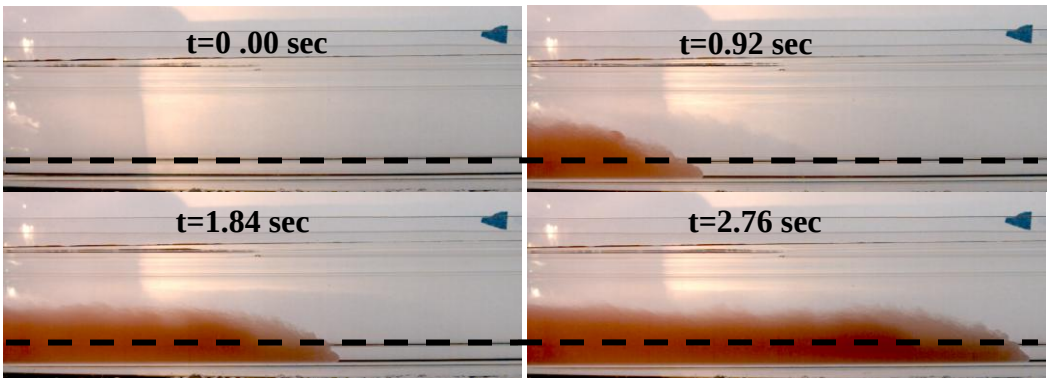

Figure 14: Progression of Gravity Currents and Stratified Flow in Case B. The Dashed Line Signifies the Inner Pipe Location

In both cases the density ratio was 0.88, which means that the brine solution is about 13% heavier than the water which is approximately, in scaled terms, the same difference as air entering from the reactor containment area into the helium coolant would be. As shown in Figs. 13 and 14, the wave front rapidly propagates through the coaxial pipe, occupying about one-half of the pipe diameter (H in Fig. 4). Both cases have turbulence clearly present. This is expected with Case A with a Reynolds number range of 0-19563 and in case B with a Reynolds number ranges of 0-18330. Also, these visualizations show formations of billows (noted in Fig.13). As previously discussed billows are type of instabilitiy that causes mixing and with further investigaion may be classified as Kelvin-Helmholtz billows due to definition given prior.

Figure 15 shows the initial rapid burst that Simpson discussed after the gate is removed indicated from the velocity jumping from 0 to 0.24 m/s and rapidly decelerating to constant velocity after the initial 0.07 meters of travel. At this point,

phase one is initiated as seen with the nearly constant velocity as the fluid propagates in the axial direction.

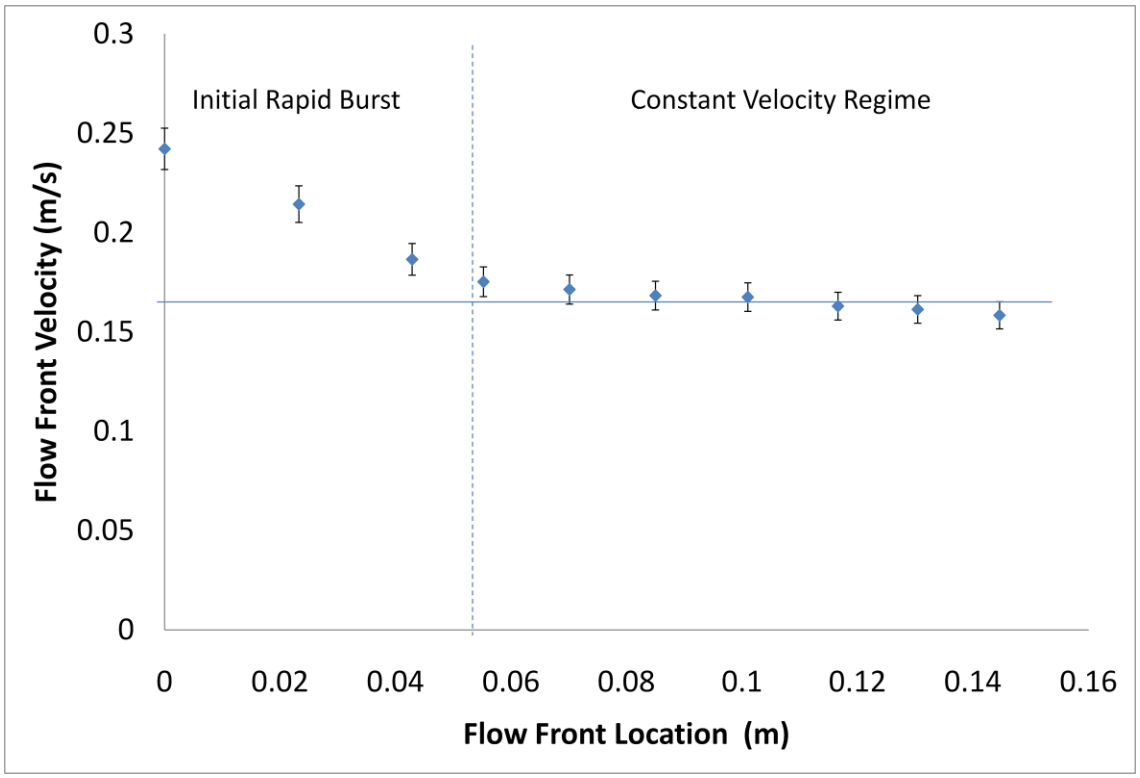

Figure 15: Experimental Results for the Pipe Flow Front Velocity versus Location in Case A

Figure 16 shows the same initial burst for Case B.

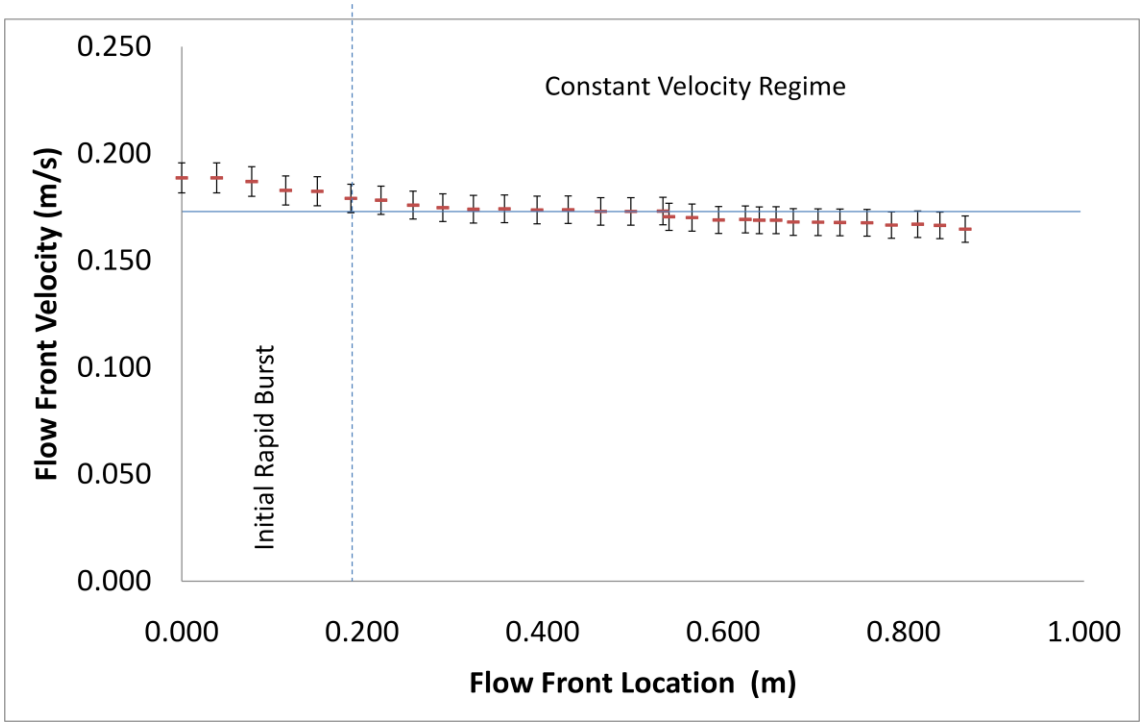

Figure 16: Experimental Results for the Pipe Flow Front Velocity versus Location in Case B

The heavy flow front velocity is consistent with the previous observations reported for the lock exchange flow in the Boussinesq flow regimes following Benjamin's equation [9], Eq. 2. In both previous evaluations, the theoretical heavy flow front velocity was estimated to be ~0.1608 m/s from Benjamin's equation. The velocities are the same for both previous evaluations due to the dependence of Benjamin's equation on the diameter only of the pipe and not on the break location.

Table 4 shows the comparison of the flow front velocities between the current experimental values and Benjamin's theoretical value. In both Case A and Case B, the

experimental front velocities are in good agreement with Benjamin's theoretical calculation (within estimated measurement uncertainty).

Table 4: Comparison of Flow Front Velocity between Experimental and Benjamin's Theoretical Model

Flow Front Velocity (m/s)		
	Case A	**Case B**
Experimental	0.164 ± 4.29%	0.168 ± 3.69 %
Benjamin's Theory	0.1608	0.1608
Error (%)	1.99	4.5

Another part of this experiment was to gain confidence in the CFD calculations by comparison with the experimental values obtained. Table 5 shows the comparison of the flow front velocities between experimental and CFD results. At this time only CFD results for case A have been completed. The flow front velocity difference is low when comparing experimental and CFD results. Therefore, it presents that the CFD model is adequately simulating the phenomenon in this lock exchange density driven stratified flow.

Table 5: Comparison of Flow Front Velocity between Experimental and CFD

Flow Front Velocity (m/s)		
	Case A	**Case B**
Experimental	0.164 ± 4.29%	0.168 ± 3.69 %
CFD	0.17	TBD
Difference (%)	3.5	NA

Flow front velocity and spreading rate measurements were conducted using high speed cameras and image processing software. Further analysis was done to measure change in position of the flow front relative to time and it's velocity as a function of position. Case A used one camera for the pipe location and one to investigate the lower plenum (125 frames per second). Case B used two cameras for the pipe location (250 fps and 300 fps) and one to investigate the lower plenum (150 fps). Flow front velocity measurements were conducted with the image processing software by using the simple equation seen in Eq. (9):

$$V=\frac{dx}{dt} \tag{9}$$

Distance of the investigation area was measured prior to the experiment and the frame rate is known. Using the image processing software pixels were correlated to distance covered in a time stamp. This time stamp was calculated by the frame rate of each camera. The results are seen in Figure 17.

According to Fig. 17, after the initial burst, the flow front location progresses linearly with time for both cases. This linear relation of flow front location with time indicates a constant heavy flow front speed axially through the coaxial pipe. This phenomenon was also observed and documented by Benjamin in his investigation of heavy salt water solution displacing the lighter fluid, water [9]. Simpson [14] shows this constant velocity is also believed to be the first phase of a lock exchange flow after the initial gate removal. Figure 17 shows a constant flow front velocity indicating steady flow conditions.

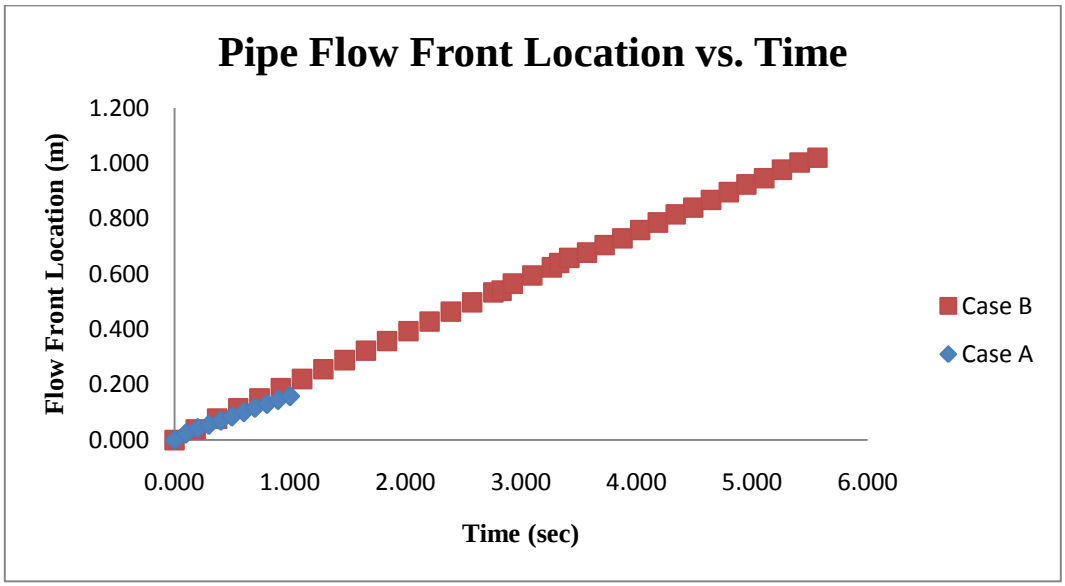

Figure 17: Experimental Results for the Pipe Flow Front Location versus Time

As it exits the pipe, the flow moves into the lower plenum of the reactor cavity. Figure 18 shows the dense fluid (simulated air ingress into reactor core) propagating into

the lower plenum from the coaxial pipe. In Fig. 18, the camera is positioned above the lower plenum and ingress through the hot duct is indicated by flow arrow.

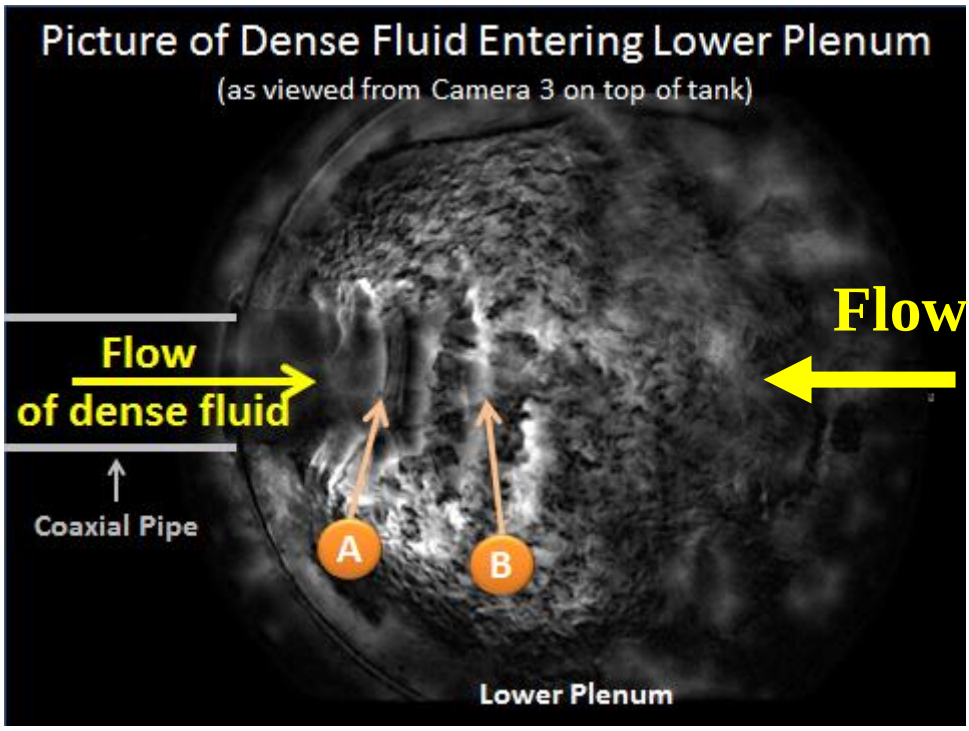

Figure 18: Highly Periodic Interfacial Instabilities between the Brine and Water

Following the initial break, the gravity driven flow spreads into the lower plenum, creating Kelvin-Helmholtz instabilities at the interface between the heavy and light flows just after the entrance region. The initial folding of waves is indicated by ‘A’ in Fig. 18, which eventually leads to a breaking wave at point ‘B.’ In addition to the

formation of a breaking wave pattern, rib vortices are formed transverse to the waves and move outward towards the edges of the wave as it propagates.

From this wave propagation, similar calculations were conducted for flow into the lower plenum of both cases. These are seen in Figs. 19 and 20. Figure 18 shows how the fluid enters the lower plenum and spreads at a constant velocity. This is the outcome of both Case A and B.

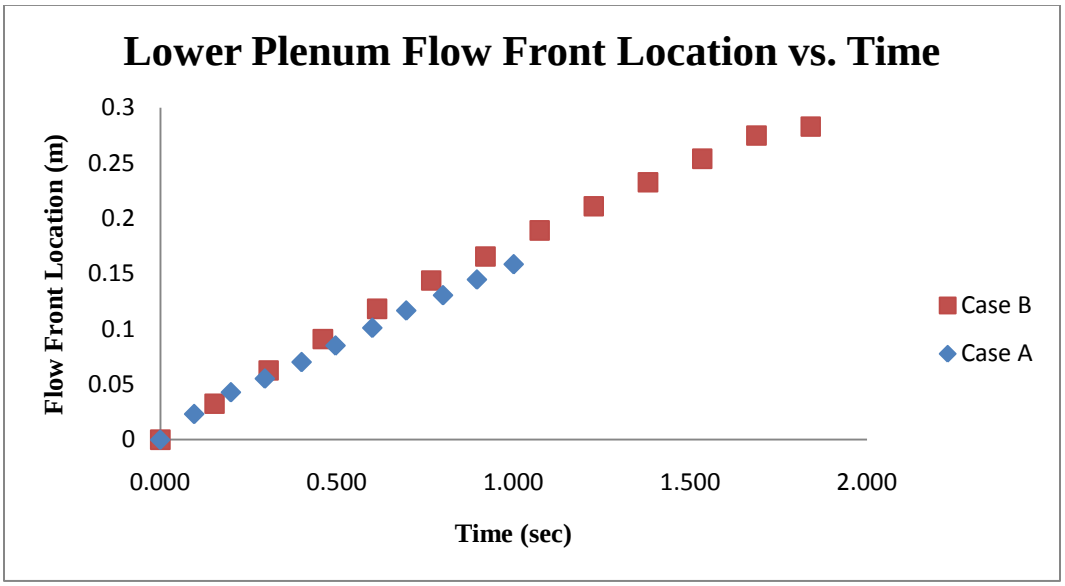

Figure 19: Experimental Results for Flow Front Location versus Time of the Lower Plenum

The same shape can also be seen in the lower plenum as in the pipe as seen in Fig. 20. The flow goes from a smaller area into a larger area creating an initial burst of

speed and then the spreading rate becomes relatively constant as it moves through the tank.

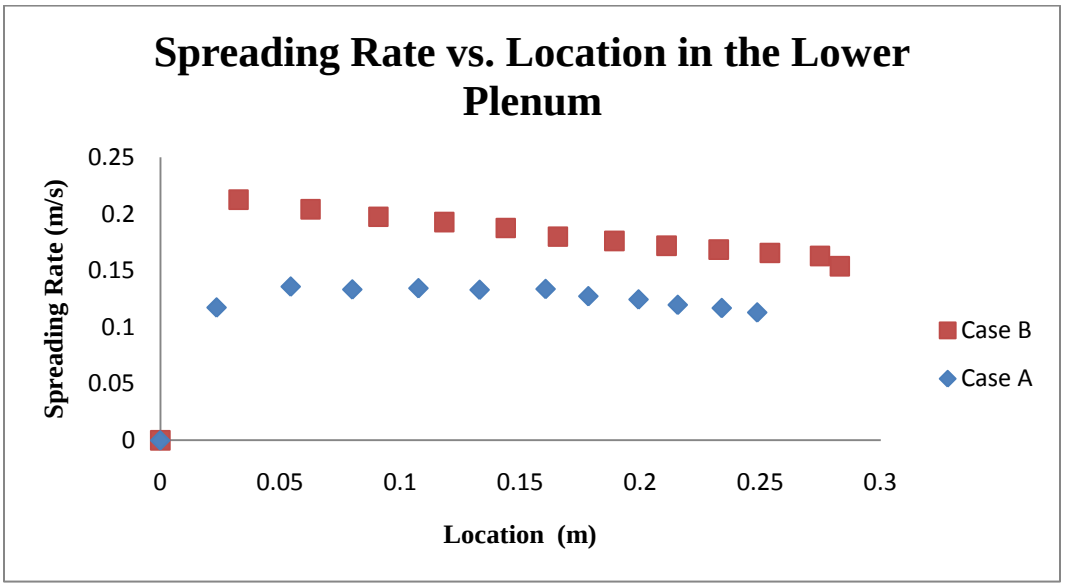

Figure 20: Experimental Results for Spreading Rate versus Location in the Lower Plenum

The time it takes for the flow to reach the lower plenum is a very short time period for both investigations. For case A the heavy brine solution reaches the lower plenum in 3.04 seconds and for case B it takes 5.2 seconds. This short timescale reveals the short mitigation time that is avalable if this event were to occur.

7.2 Gas-gas Air Ingress Investigation

PIV investigations have been initiated to analyze the flow front of the gas-gas scenarios. Currently the first PIV tests have been conducted with SF_6 as the heavy working fluid and helium as the light. Zinc stearate particles are used as the chosen seeding particles to follow the SF_6 gas due to their relatively light density and particle distribution which can be seen in the next section.

In order to compare the velocity and time scale of density driven stratified flow from PIV data, diffusion time scale and diffusion velocity was calculated. Diffusion time scale and velocity was calculated for both gas scenarios, SF_6/He and CO_2/He. The SF_6/He gas case is the only comparison available at this time since the CO_2/He gas case has not been run at this time. Equation 10 is the equation used to calculate the binary diffusion coefficient [18]. Equation 11 and 12 gives the diffusion time scale and diffusion velocity respectively.

$$D_{SF6\text{-}He} = \frac{2.628 \times 10^{-7} T^{3/2}}{(P\sigma^2_{SF6\text{-}He}\Omega_D M^{1/2}_{SF6\text{-}He})} \tag{10}$$

$$t_{Diff} = \frac{L^2}{D_{SF6\text{-}He}} \tag{11}$$

$$V_{Diff} = \frac{L}{t_{Diff}} \tag{12}$$

The diffusion time and diffusion velocity are compared to the experimental values of the density-driven stratified flow front. These values can be seen in Table 6.

The heavy flow front of the density-driven stratified flow was measured from the PIV data. This velocity is two orders of magnitude larger than the diffusion velocity. This shows the differing importance of the two mechanisms and the reason density-driven stratified flow needs to be investigated.

Table 6: Comparison of Diffusion Velocity to Density-driven Stratified Flow

	SF6-He	CO2-He
t_{Diff} (s)	195.4	141.1
V_{Diff} (m/s)	0.0046	0.0063
u_{Heavy} (m/s)	0.31	----

7.2.1 PIV Seeding Analysis

An important factor in PIV is the ability of the seeding particles, or tracer particles, to move with the flow. Thus, the selection of particles is key to ensure an accurate representation of the flow features present in the air ingress scenario. Zinc stearate seeding particles were chosen based on particle size distribution and density. The average particle size is ~2 μm with a density of 400 kg/m^3.

It is important to ensure that particles are the particular size obtained from the manufacturers. Normally a manufacturer gives the particle diameter according to the largest particle diameter but not the distribution. It is important to know the distribution of the particles to ensure the correct particles are chosen.

Particle size distributions of various manufacture samples were performed using a TSI Aerodynamic Particle Sizer (APS model number 3321) to ensure the particles

adhered to the manufacturer specifications. The particle size distributions of two manufacturers, Ferro and Struktol, are presented in Figs. 21 and 22 respectively. It can be seen that the zinc stearate particles from the Ferro manufacturers has a more consistent distribution with a peak approximately at 1.7 micrometers. Figure 22 shows a less consistent distribution with bi-modal distribution with peaks present at 0.8 and 1.7 micrometers. From this particle analysis of these two particles, Ferro, the more consistent particle distribution is chosen as the particles to use in the investigation.

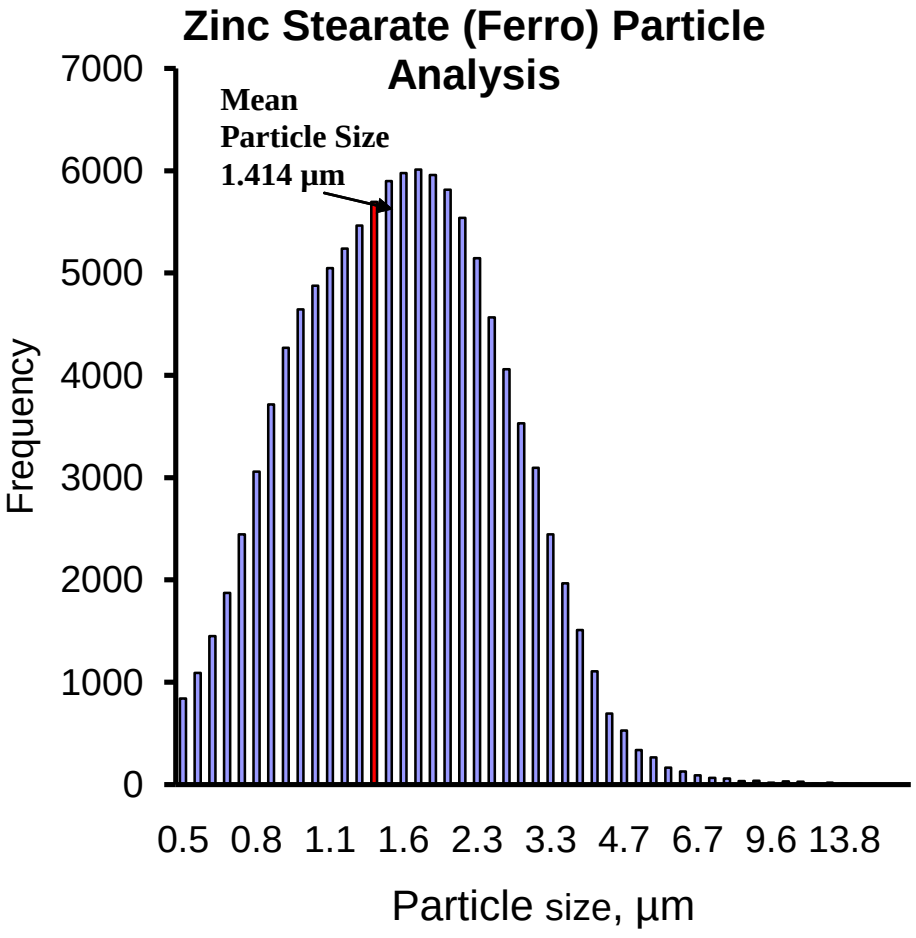

Figure 21: Zinc Stearate Particle Analysis (Ferro)

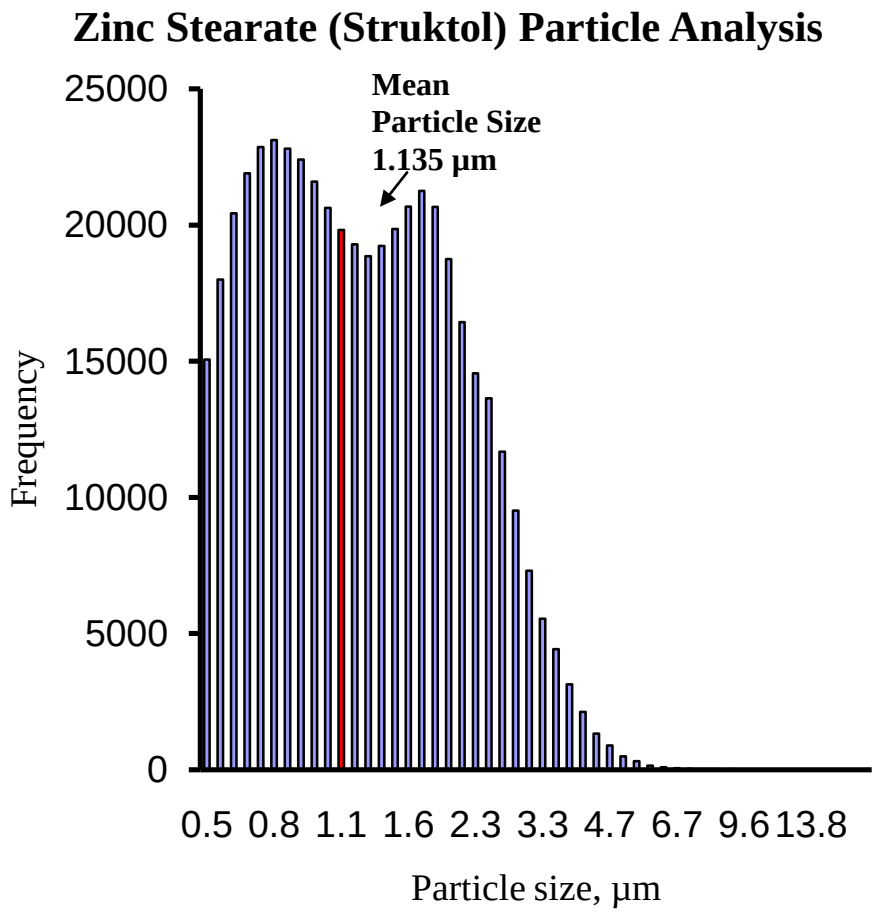

Figure 22: Zinc Stearate Particle Analysis (Struktol)

8. FUTURE WORK

Future work will include more detailed investigations of the gas to gas cases that are presented. This will include furthering investigations with current SF_6 and He to look at different areas of areas of interest of the pipe location. Another interest will be incorporating Laser Induced Fluorescence (LIF) to capture full-field velocity concentration profiles of the gases used in addition to the current PIV. Hot-wire anemometers will also be inserted into the duct and the tanks to obtain local velocity values to correlate back to the PIV data for validation. Once these investigation techniques are employed in the first gas case, and then the other gas case, carbon dioxide and helium, presented in Table 1, will be investigated in order to obtain a full catalog of information regarding this accident scenario.

9. SUMMARY AND CONCLUSIONS

Due to the differing time scales of interaction, the air ingress mechanism, whether it is dominated by diffusion or density-driven stratified flow need to be verified. Air ingress could possibly result in oxidation of in-core graphite structures and fuel, potentially collapsing the bottom structures of the core and releasing fission products and hazardous levels of carbon monoxide [2]. The shorter the time scale indicated by the density driven stratified flow causes a faster onset of natural circulation leading to earlier graphite oxidation. This earlier onset of oxidation provides less time for outside mitigation.

From the experimental investigation, the gravity driven ingress mechanism is verified as being a shorter time scale by using selected fluids. Brine was used as the heavy fluid and water as the light with a density ratio of 0.88. The experiment shows stratification of the two fluids. The flow front analysis for the coaxial pipe is in agreement with Benjamin's theoretical value and with CFD results.

The time it takes for the flow to reach the lower plenum is a very short time period for both investigations. Both cases results in the heavy fluid entering the lower plenum in under 6 seconds. This short timescale reveals the short mitigation time that is avalable if this event were to occur.

The diffusion velocity and heavy flow front of the stratified flow layer were compared for the SF_6/He gas case. It is seen that the diffusion plays less of a role as the transport mechanism in comparison to the density-driven stratified flow since the

velocity of the diffusion is two orders of magnitude smaller than the velocity of the stratified flow mechanism. This is the reason for the need for density-driven stratified flow investigations following a LOCA.

REFERENCES

[1] U.S. DOE Nuclear Energy Research Advisory Committee and the Generation IV International Forum, 2002, "A Technical Roadmap for Generation IV Nuclear Energy Systems," Generation IV International Forum.

[2] Oh, C. H, Kim, E. S., NO, H. C, Cho, N. Z., 2008 "Experimental Validation of Stratified Flow Phenomena, Graphite Oxidation, and Mitigation Strategies of Air Ingress Accidents," INL/EXT-08-14840, Idaho National Laboratory, Idaho Falls, ID.

[3] Oh, C., Davis, C., Siefken, L., Moore, R., NO, H., Kim, J., Park, G.C., Lee, J., and Martin, W., 2006, "Development of Safety Analysis Codes and Experimental Validation for a Very High Temperature Gas-Cooled Reactor," Final Report, INL/EXT-06-01362, Idaho National Laboratory, Idaho Falls, ID.

[4] Oh, C., Kim, E., Schultz R., Petti D., 2009, "Computational Fluid Dynamics Analyses on Very High Temperature Reactor Air Ingress," ICONE 17-75863 *17th International Conference on Nuclear Engineering*, July 12-16, Brussels, Belgium.

[5] Oh, C. H, Kim, E. S., Schultz, R., Petti, D., and Liou, C. P., 2008, "Implications of Air Ingress Induced by Density-Difference Driven Stratified Flow," 8023, *International Congress on Advances in Nuclear Power Plants*, pp. 313-322.

[6] Schultz, R., Nigg, D., Johnson, R., Oh, C., Johnsen, G., 2006, "Next Generation Nuclear Plant Methods Technical Program Plan," INL/EXT-06-11804, Rev 0.26, Idaho National Laboratory, Idaho Falls, ID.

[7] Williams, B., Liou, C., Schultz, R., Kadakia, H., Phoenix, B., Horrocks, D., 2007, "Providing the Basis for Innovative Improvements in Advanced LWR Reactor Passive Safety Systems Design: An Educational R&D Project," Idaho State Univ. Pocatello, ID, Final Report-DE-FG07-03ID14500.

[8] Oh, C. H and Kim, E. S, 2010, "Isothermal Air Ingress Validation Experiments at Idaho National Laboratory: Description and Summary of Data," INL/EXT-10-19727, Idaho National Laboratory, Idaho Falls, ID.

[9] Benjamin, T. B., 1968, "Gravity Currents and Related Phenomena," J. Fluid Mechanics, **31**, pp. 209–248.

[10] Duncan, J. B., and H. L. Toor, 1962, "An Experimental Study of Three Component Gas Diffusion," A.I.Ch.E. Journal, **8**, pp. 1-38.

[11] Lakehal, D., Lemonnier, H., 2003, "Test-case Number 28: The Lock-Exchange Flow," Nuclear Engineering Laboratory, Zurich, Switzerland, March 17, 2003.

[12] Shin, J.O., Dalziel, S. B., Linden, P.F., 2004, "Gravity Currents Produced by Lock Exchange," J. Fluid Mech. **521**, pp. 1-34.

[13] Simpson, J. S., 1997, "Chapter 11: The Anatomy of a Gravity Current and Chapter 12 Spread of Dense Fluid," *Gravity Currents in the Environment and the Laboratory*, 2nd Edn. Cambridge University Press, Cambridge, UK.

[14] Turner, J.S., 1973, *Buoyancy Effects in Fluids*, Cambridge Monographs on Mechanics and Applied Mathematics. Cambridge University Press, Cambridge, UK, pp. 70–74.

[15] Parsons, J., "Conservative Gravity Currents," Ocean Engineering, University of

Washington, Seattle, WA.

[16] Adrian, R., 1991, "Particle-Imaging Techniques for Experimental Fluid Mechanics," Annu. Rev. Fluid Mech., **23**, pp. 261-304.

[17] Riethmuller, M.L., 2000, "Particle Image Velocimetry and Associated Techniques," von Karman Institute for Fluid Dynamics, Genese, Belgium.

[18] Annamalai, K. and Puri, I.K., 2007, "Chapter 6: Mass Transfer," *Combustion Science and Engineering*, CRC Press, Boca Raton, FL.

VITA

Name: Jessica Lauren Hartley

Address: Department of Mechanical Engineering

c/o Dr. Yassin Hassan

Texas A & M University

College Station, TX 77843-3133

Email Address: jlhartley8@gmail.com

Education: B.S., Mechanical Engineering, West Texas A&M University, 2009

M.S., Mechanical Engineering, Texas A&M University, 2011